



1 **Aerosol absorption retrieval at ultraviolet wavelengths in a 2 complex environment**

3

4 **Stelios Kazadzis^{1,2}, Panagiotis I. Raptis², Natalia Kouremeti¹, Vassilis Amirdidis³,
5 Antti Arola⁴, Evangelos Gerasopoulos², Gregory L. Schuster⁵**

6 [1] {Physikalisch-Meteorologisches Observatorium Davos, World Radiation Center
7 (PMOD/WRC) Dorfstrasse 33, CH-7260 Davos Dorf, Switzerland}

8 [2] {Institute of Environmental Research and Sustainable Development, National Observatory
9 of Athens, Greece}

10 [3] {Institute of Astronomy Astrophysics, Space Applications and Remote Sensing, National
11 Observatory of Athens, Greece}

12 [4] {Finnish Meteorological Institute, Kuopio Unit, Finland}

13 [5] {NASA Langley Research Center, Hampton, VA, USA}

14 Correspondence to: stelios.kazadzis@pmodwrc.ch

15

16 **Abstract**

17 We have used total and diffuse UV irradiance measurements with a multi-filter rotating
18 shadow-band radiometer (UVMFR), in order to calculate aerosol absorption properties
19 (Single Scattering Albedo - SSA) in the UV range, for a 5 years period in Athens, Greece.
20 This data set was used as input to a radiative transfer model and the SSA for 368nm and
21 332nm has been calculated. Retrievals from a collocated CIMEL sun-photometer were used
22 to validate the products and study absorption spectral behavior SSA values at these
23 wavelengths. UVMFR SSA together with synchronous,CIMEL-derived, retrievals at 440nm,
24 show a mean of 0.90, 0.87 and 0.83, with lowest values (higher absorption) towards lower
25 wavelengths. In addition, noticeable diurnal variations of the SSA in all wavelengths are
26 revealed, with amplitudes in up to 0.05. High SSA wavelength dependence is found for cases
27 of low Ångström exponents and also an SSA decrease with decreasing extinction optical



1 depth, suggesting an effect of the different aerosol composition. Dust and Brown Carbon UV
2 absorbing properties were investigated to understand seasonal variability of the results.

3

4 1 Introduction

5 The role of aerosols, both natural and anthropogenic, is extremely important for regional and
6 global climate change studies as well as for overall pollution mitigation strategies (e.g.
7 IPCC, 2013). However, a considerable amount of work still needs to be carried out,
8 particularly as it appears that climate change is accelerating with aerosols impacting at local,
9 regional and global scales. Furthermore, the components controlling aerosol forcing, account
10 for the largest uncertainties in relation to anthropogenic climate change (IPCC, 2007, IPCC,
11 2014). A comprehensive review of the assessment of the aerosol direct effect, its state of play
12 as well as outstanding issues, is given by (IPCC, 2014) and (Yu *et al.*, 2006). Both emphasize
13 that the significant aerosol absorption uncertainties in global Single Scattering Albedo (SSA),
14 constitute one of the largest single source of uncertainty in current modeling estimates of
15 aerosol climate forcing. SSA is the ratio of scattering to total extinction (scattering plus
16 absorption), and it depends strongly on chemical composition, particle size, mixture, relative
17 humidity and wavelength. Comprehensive measurements are crucial to understand their
18 effects and to reduce SSA uncertainties that propagate into aerosol radiative forcing estimates.
19 For example for the same aerosol load (aerosol optical depth), the absorbing nature of
20 aerosols can lead to up to 50% change in the erythermal irradiance, compared to only
21 scattering aerosols (Bais *et al.*, 2014). SSA calculated here differs from in situ SSA values
22 retrieved from absorption and scattering measurements at a single altitude level (e.g. at the
23 ground), in that it is a columnar measurement, arising from solar irradiance attenuation along
24 a fixed irradiance path.

25 In the visible (VIS) part of the spectrum, advanced retrieval algorithms for microphysical
26 aerosol properties have been developed in the framework of the Aerosol Robotic Network
27 (AERONET) and the Skyradiometer Network (SKYNET) (*e.g.*, Dubovik and King, 2000;
28 Nakajima *et al.*, 1996) All AERONET stations currently provide inversion based VIS-SSA
29 retrievals. In addition, Goering *et al.* (2005), Taylor *et al* (2008) and Kudo *et al.* (2008) have
30 proposed estimation techniques for the retrieval of spectral aerosol optical properties by
31 combining multi-wavelength measurements using a priori constraints that are applied
32 differently than in the single wavelength methods. SSA retrieval in the ultraviolet (UV) part



of the spectrum is weaker with large uncertainties. As AERONET does not provide any information about SSA at the UV, compared to the visible spectral region, only a few publications have dealt with aerosol absorption at UV wavelengths (e.g. Eck et al., 1998; Krotkov et al., 2005a; Bais et al., 2005; Corr et al., 2009). It is envisaged that improvement in measurement precision and in the general understanding of aerosol absorption in the UV (and immediate derivatives like the SSA) in various scientific applications, will contribute significantly to enhancing the accuracy of radiation forcing estimates. For example, desert dust particles (Alfaro et al., 2004), soot produced by fossil fuel burning, and urban transportation, all strongly absorb UV radiation. However, optical properties of other potential UV absorbers like organic, nitrate and aromatic aerosols are still poorly known. Bergstrom et al., 2003 showed that spectra of aerosol SSA obtained in different campaigns around the world differed significantly from region to region, but in ways that could be ascribed to regional aerosol composition. Moreover, results from diverse air, ground, and laboratory studies, using both radiometric and in situ techniques, show that the fractions of black carbon, organic matter, and mineral dust in atmospheric aerosols play a role in the determination of the wavelength dependence of aerosol absorption (Russell et al., 2010). Barnard et al. (2008), investigating the variability of SSA in a case study for the Mexico City metropolitan area, found that, in the near-UV spectral range (250 to 400 nm), SSA is much lower compared to SSA at 500 nm indicative of enhanced absorption in the near-UV range. They suggested that absorption by elemental carbon, dust or gas alone could not account for this enhanced absorption leaving the organic carbon component of the aerosol as the most likely absorber. It has been found in many studies that, in addition to dust, the absorbing organic carbon compounds can induce strong spectral absorption increasing towards the shortest UV wavelengths. Sources of these light-absorbing organic carbon compounds (often called as "Brown Carbon", BrC) are various; biomass burning (e.g. Kirchstetter et al. 2004), urban smoke (e.g. Liu et al. 2015) and biogenic emissions (e.g. Flores et al. 2014).

Moosmuller et al (2012) showed that iron concentration in mineral dust aerosols is linked to lower SSA at 405nm than in 870, which could be a hint for lowest SSA in the UV-VIS range during dust events. Medina et al (2012) found in El Paso-Juarez also large variation in UV range SSA, with lower values than visible wavelengths and showed that on heavy polluted days it can get as low as 0.53 at 368nm. An effort was made to calculate SSA in lower UV wavelengths, using Brewer measurements, at Belgium, revealing lowest values but with high uncertainty (Nikitidou et al, 2013). Recently Schuster et al (2016) have tried to distinguish



1 aerosol types, by their optical properties and assumed that dust particles have higher
2 absorption at UV wavelengths, and used imaginary refractive index spectral dependence to
3 separate from black carbon and infer hematite/goethite in the coarse mode. They found that
4 dust particles containing hematite are highly absorbing in the UV region.

5 Ultraviolet (UV) solar radiation has a broad range of effects on life on Earth (UNEP et al.,
6 1998;UNEP et al., 2007;UNEP, 2003). It influences not only human beings (e.g. (Diffey,
7 1991)), but also plants and animals (e.g. Bornman and Teramura, 1993). Furthermore, it
8 causes degradation of materials and functions as a driver of atmospheric chemistry. There are
9 various studies linking changes of the UV radiation field with changes in the scattering and
10 absorption of aerosols in the atmosphere (e.g. Zerefos et al., 2012). Such changes can be
11 comparable in magnitude with those caused by the decline in stratospheric ozone (Elminir,
12 2007; Reuder and Schwander, 1999; Krotkov et al., 1998). As an example, analysis of long
13 term UV time series at Thesaloniki, Greece, showed a reduction of 7% of AOD per decade
14 was recorded, but the UV Irradiance has increased by 9% (after removing ozone column
15 effect on it) which could only be explained by change in the absorption characteristics of
16 aerosols in the area (Meleti et al, 2009). Moreover, UV variations caused by changes in
17 aerosol optical properties directly affect tropospheric photochemistry:

- 18 - increases in regional O₃ (10-20 ppb for Eastern USA) caused by increased UV levels
19 due to the presence of non-absorbing aerosols (Dickerson et al., 1997).
20 - decreases in regional O₃ (up to 50 ppb for Mexico City and for particular days) caused
21 by strong UV reduction due to absorbing aerosols (Castro et al., 2001).

22 There are also several more scientific issues that may be clarified with accurate knowledge of
23 aerosol absorption properties:

- 24 • *Aerosol effects on UV trends may enhance, reduce or reverse effects of stratospheric
25 ozone change*

26 Future scenarios for simulations of global UV levels are based on ozone recovery, having as
27 their sole input the predicted future decline in columnar ozone. Furthermore, simulations of
28 observed tendency of reduced anthropogenic aerosols in the atmosphere in the US and Europe
29 during the course of the last decade (den Outer et al., 2005) included only cloud and AOD
30 changes in the characterization of likely UV trends. In this regard, changes in the absorbing
31 properties of aerosols on global scales would have had a large effect on the uncertainty budget



1 in any of the above simulations (WMO, 2003). For example, a decrease in aerosol absorption
2 properties accompanied by an AOD decrease in Europe could lead to a significant
3 acceleration of the calculated ozone decline related to UV upward trends (Kazadzis et al.,
4 2009, Zerefos et al., 2012).

- 5 • *Solar irradiance satellite retrieval algorithms are directly affected by the presence of*
6 *absorbing aerosols*

7 The discrepancies between ground-based (GB) UV measurements and satellite-derived (OMI,
8 TOMS, GOME) data are directly related to aerosol absorption that is absent from satellite
9 retrieval algorithms (Tanskanen et al., 2007; Arola et al., 2005). It has been shown that
10 enhanced aerosol UV absorption in urban areas can cause up to 30% overestimation in the
11 satellite retrieved UV radiation (Kazadzis et al., 2009).

- 12 • *Uncertainty on commonly used atmospheric radiative transfer applications and codes*

13 Radiative transfer algorithms calculating UV irradiance, fall short in precision due to large
14 uncertainties in the input parameters (e.g. levels of ozone, aerosol composition and the surface
15 albedo) used in model calculations. It is now known that the major input source of uncertainty
16 in radiative-transfer model simulations, is aerosol absorption (e.g. Van Weele et al., 2000). In
17 particular, the direct radiative effect of aerosols is very sensitive to SSA. For example, a
18 change in SSA from 0.9 to 0.8 can often alter the sign of the direct effect (Yu et al., 2006).
19 Furthermore, availability and quality of observational SSA data do not match with those
20 available for AOD (Krotkov et al., 2005a). This is compounded by the lack of information on
21 the vertical profile of aerosol optical properties such as the SSA at global scales. Only few
22 case studies have dealt with such measurements and have been limited to local scales (Müller
23 et al., 1999).

24 a. The major parameters that describe radiation and aerosol interactions are the aerosol
25 optical depth (τ), the SSA and the asymmetry parameter (g). The aerosol optical depth at a
26 wavelength λ is the integral of the aerosol extinction coefficient ($b_{ext}(\lambda)$) over a certain
27 atmospheric layer (in the height range z_1 to z_2).

28 b.

29
$$\tau = \int_{z_1}^{z_2} b_{ext}(\lambda) \cdot dz \quad (1)$$



1 The SSA at a wavelength λ provides the contribution of aerosol particle scattering relative to
2 the total extinction (absorption plus scattering),

3
$$\text{SSA} = \frac{b_{sca}(\lambda)}{b_{abs}(\lambda) + b_{sca}(\lambda)} \quad (2)$$

4 Values for the SSA range from 0 (absorbing aerosols only) to 1 (no absorption). The
5 asymmetry parameter, is the phase function (P) weighted average of the cosine of the
6 scattering angle (θ) over all directions. Assuming azimuthal symmetry, the scattering angle
7 integration extends from $-\pi$ to $+\pi$ such that the asymmetry parameter (g) is given by

8
$$g = \frac{1}{2} \cdot \int_{-\pi}^{\pi} \cos\theta \cdot P(\theta) \cdot \sin\theta \cdot d\theta \quad (3)$$

9 Values for g range from -1 (backscattered radiation only) to 1 (forward scattered radiation
10 only) in theory, and from 0 to 1 for particles in the atmosphere.

11 Corr et al. (2009) presented a review of studies estimating SSA at different wavelengths. For
12 the visible part of the spectrum, two different approaches have been presented. The first
13 (Dubovik et al., 2002), introduced sky radiance measurements in a matrix inversion technique
14 to calculate various aerosol microphysical properties. This methodology has been widely
15 applied in the AERONET. The second (Kassianov et al., 2005), proposed the use of radiative
16 transfer model (RTM) calculations, using as input measurements of AOD and the ratio of
17 direct to diffuse irradiance at specific wavelengths. However, in the case of SSA calculations
18 at UV wavelengths, enhanced measurement uncertainties, RTM input assumptions, and
19 interference of absorption by other gases (O_3 , NO_2), make the retrieval more difficult. All
20 reported results concerning UV-SSA, utilize RTM combined with total and diffuse relative
21 irradiance measurements (Herman et al., 1975; King and Herman 1979; King 1979; Petters et
22 al., 2003; Krotkov et al., 2005b; Corr et al., 2009; Bais et al., 2005) or absolute irradiance
23 measurements (Kazadzis et al., 2010; Ialongo et al., 2010; Bais et al., 2005). The review made
24 by Corr et al. (2009) also presents the major differences in the results of simulations of the
25 SSA, arising from RTM input assumptions, measurement techniques and retrieved
26 wavelengths. An additional problem is that previous studies have dealt with short time periods
27 due to the limited lifespan of experimental campaigns.

28 In this work, for the calculation of the UV-SSA, we adopt a methodology based on the idea of
29 Krotkov et al. (2005a), Krotkov et al. (2005b) and Corr et al. (2009). The methodology,
30 together with the retrieval tools used and technical assumptions made are presented in section



1 2. Results of UV-SSA measurements and their comparison with synchronous AERONET
2 retrievals in the visible range are presented in section 3. Finally, discussion of the observed
3 diurnal SSA patterns in Athens, SSA wavelength dependency as well as overall conclusions
4 are presented in the last section of this work.

5

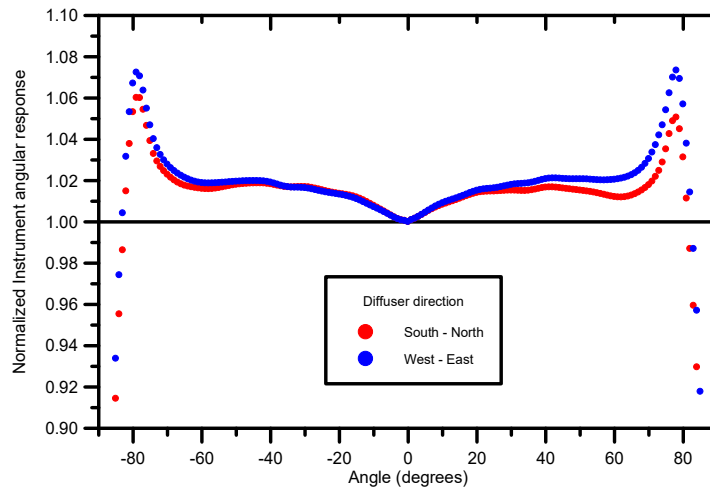
6 **2 Instrumentation and retrieval methodology**

7 **2.1 Instrumentation**

8 In this work we present estimates of SSA at two independently retrieved UV wavelengths
9 332nm and 368 nm for an urban site situated in Athens, Greece. The period of measurements
10 analysed is from July 2009 to May 2014. Since February 2009, the ground-based
11 Atmospheric Remote Sensing Station (ARSS) has been in continuous operation to monitor
12 ground radiation levels and aerosol loadings over Athens (Amiridis et al., 2009). ARSS is
13 located on the roof of the Biomedical Research Foundation of the Academy of Athens (37.9
14 N, 23.0E, 130 m a.s.l.) (<http://apcg.meteo.noa.gr/index.php?option=112&client=&langid=2>)
15 and the campus is located near the city centre, 10 km from the sea (Gerasopoulos et al., 2009).
16 The horizon view is clear at 360 degrees viewing angle. ARSS is equipped with a CIMEL
17 CE318-NEDPS9 sun photometer for the retrieval of AOD at 8 wavelengths in the range of
18 340nm to 1640 nm, including polarization measurements as part of NASA's AERONET
19 (<http://aeronet.gsfc.nasa.gov>). The technical specifications of the instrument are given in
20 detail by Holben et al. (1998). ARSS is also equipped with an Ultraviolet Multi-filter
21 Radiometer (UVMFR) instrument for radiation measurements in the UV spectral region
22 (Harrison et al., 1994). UVMFR measures both total and diffuse irradiance at 7 specified
23 wavelengths (300, 305.5, 311.4, 317.6, 325.4, 332.4, and 368 nm) with a 2 nm nominal full
24 width at half maximum (FWHM) bandwidth. The instrument has been purchased on
25 November 2009 and the constructing company (Yankee Environmental Systems, USA) has
26 provided angular, spectral and absolute response functions of each wavelength channel of the
27 instrument that were measured at the National Institute of Standards and Technology (Figure
28 1). For the analysis included in this work we assume that the effective wavelengths for each
29 channel were stable during the whole period. Measurements of total and diffuse irradiance are
30 recorded every 10 seconds, and stored as 1 minute averages along with a computation of the
31 direct irradiance. Measurement data were angle-corrected, calibrated and analysed via the



1 YESDAS Manager software. The individually characterized cosine response, supplied with
2 each instrument, was used by system software to correct, in real time, for deviations from the
3 ideal cosine response (Harrison et al., 1994). For this work, we have used measurements of
4 the two aforementioned instruments in conjunction with radiative transfer model (RTM)
5 calculations that have been performed using the Libradtran code (Mayer and Kylling, 2005).



6
7 **Figure 1.** UVMFR angular response function at 368nm channel, normalized to the ideal (cosine)
8 angular response. 2 sets of responses one from the south to north scan and one from the west to east
9 are presented.
10

11 **2.2 Retrieval methodology**

12 SSA is a key aerosol optical property and describes the portion of solar irradiance that is
13 scattered from the main direct beam passing through the atmosphere. Changes in SSA
14 influence mostly the diffuse radiation reaching the earth's surface, while its effect on direct
15 radiation can be considered negligible. SSA values in the atmosphere range from 0.5 to 1.0 at
16 visible wavelengths.
17 Model calculations can be used for retrieving SSA when global and/or diffuse spectral
18 irradiance, solar zenith angle (SZA), total column ozone, and AOD are known (Krotkov et al.,
19 2005b; Kazadzis et al., 2010; Ialongo et al., 2010; Corr et al., 2009; Bais et al., 2005). In our
20 retrieval methodology we have used partly the basic approach that is described in detail in the
21 Corr et al. (2009), Krotkov et al. (2005a) and Krotkov et al. (2005b). This approach consists
22 of measurements of the direct to global irradiance ratios (DGR) and AODs measured with the
23 UVMFR instrument for our case, that are used as basic input parameters to the RTM for the



1 calculation of the SSA at 332nm, and 368nm. These wavelengths are selected for having the
2 lowest ozone absorption from the seven available (Bass and Paur ,1985). The advantage of
3 this method is that the same detector and filter measure global and direct irradiance, thus there
4 is no need for absolute irradiance calibration and raw voltage measurements could be used.

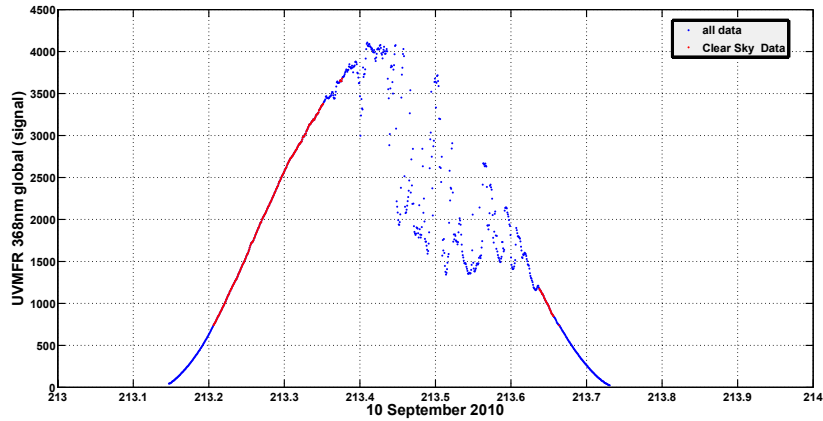
5 Global irradiance measurements from the UVMFR have been used in order to distinguish
6 cloud free conditions for each of the one minute measurements. Clouds are detectable in the
7 measured UVMFR global irradiance (GI) (at 368nm) since they cause larger variability than
8 aerosols. For distinguishing between cloudy and cloud free conditions, we have applied an
9 updated version of the method of Gröbner et al., (2001). The method is based on the
10 comparison of the measured global irradiance with radiative transfer calculations for cloud
11 free conditions and quality assurance is checked by the following criteria:

12 a. The measured GI has to lie within the modeled (cloud free) GI for a range of aerosol loads
13 (AOD at 500 nm of 0.1 and 0.8, respectively), corresponding to the 5th and 95th percentile of
14 the AERONET data for the examined location and period

15 b. The rate of change in the measured GI with SZA has to be within the limits depicted by the
16 modeled cloud free GI, otherwise the measurements are assumed cloud contamination.

17 c. All measured GI values within a time window ($dt = \pm 10$ min) should be within 5% of the
18 modeled cloud free GI, and adjusted to the level of the measurement, using an integral over
19 dt .

20 If at least 85% of the points in dt pass tests a) – c), then the central point is flagged as cloud
21 free. In this study, we have allowed a tolerance level of $\pm 10\%$ for tests a) and b) in order to
22 compensate for differences between the modeled GI and measured GI due to instrumental
23 uncertainties, as well as for usage of average climatological parameters (constant total ozone
24 column, SSA, e.t.c.) as inputs to the model. We have limited the method to $SZA < 70^\circ$ to avoid
25 uncertainties related with low solar irradiance levels. An example of the results of the method
26 is presented in figure 2 for a day with variable cloudiness. It has to be noted that in all
27 CIMEL-UVMFR comparisons, using synchronous measurements, both the above method and
28 AERONET cloud flagging algorithm are taken into account.



1

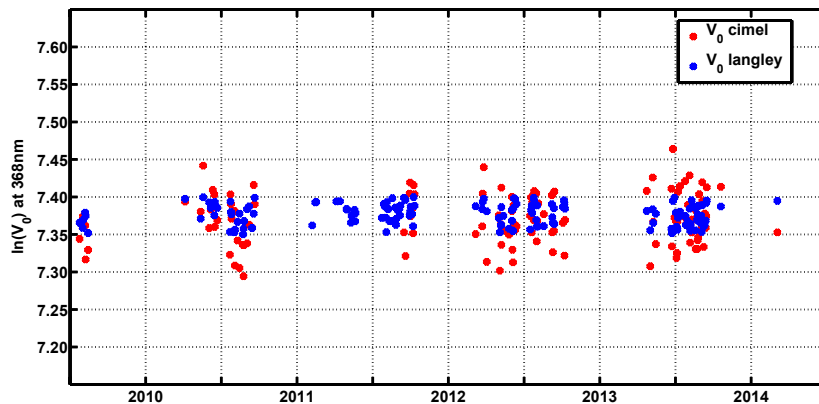
2 **Figure 2.** Determination of cloudless 1-minute measurements (red), from all measurements
3 (blue) for a day with variable cloudiness

4

5 Measurements of the diffuse and global irradiance from the UVMFR have been used in order
6 to retrieve the direct irradiance at 332nm and 368nm. We used the AERONET database to
7 select days with very low AOD (<0.1). For the urban environment of Athens such cases are
8 related with the presence of northern winds. Afterwards we selected cloudless sky half-days
9 for performing extraterrestrial Langley calibration constant (ETC) determination by applying
10 the Beer-Lambert law for UVMFR direct measurements. V_{olangley} in figure 3 represent the half
11 day values calculated with this method. In order to examine the consistency of this approach
12 we calculated the V_{0cimel} also as

$$V_{\text{0cimel}} = V e^{\mu (AOD_{\text{cimel}} + \tau_{\text{rayleigh}})}$$

13 where V is the voltage measured by UVMFR, μ is the air mass, AOD_{cimel} is the extrapolated
14 AOD at UVMFR wavelengths and τ_{rayleigh} is Rayleigh scattering optical depth. Daily averages
15 of V_{0cimel} for the selected days were compared with V_{olangley} as presented at figure 3. These
16 independent approaches appear stable through the years, with no obvious drift or change, so
17 we decided to use a single ETC for the whole period for each wavelength.



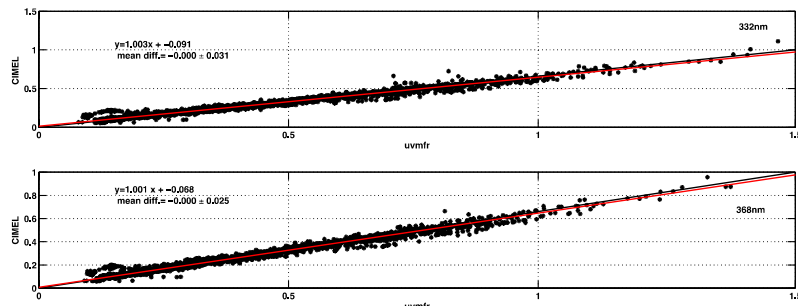
1

2 **Figure 3.** ETC values at 368nm, calculated using Langley plots of UVMFR measurements,
3 and Using Cimel extrapolated AOD's as input, for selected (low AOD's and clear sky) days
4 for the whole period

5

6 AOD's at 332 nm and 368 were calculated using the selected UVMFR derived ETC. In
7 contrast with the Krotkov et al., 2005a approach we have not transferred the CIMEL ETCs to
8 the UVMFR measurements; rather, we have independently calculated UVMFR-based AODs.
9 Validation of the results was performed based on synchronous UVMFR and CIMEL
10 measurements. The mean AOD calculated from the 1 minute UVMFR measurements within
11 ± 5 minutes from the CIMEL measurement (when the UVMFR 10 minute period is
12 characterized by cloudless conditions) has been defined as synchronous. Since the CIMEL
13 instrument provides measurements of AOD at 340 nm and 380 nm, we first calculated the
14 CIMEL derived AOD at 332 nm and 368 nm using least square quadratic spectral
15 extrapolation, using four CIMEL wavelengths (Eck et al, 1999).

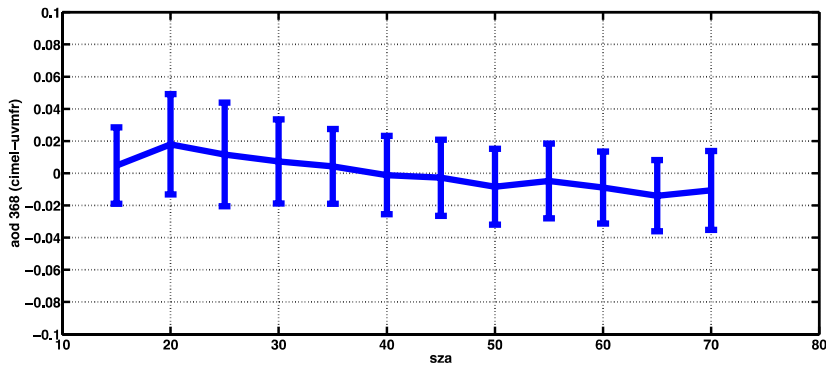
16



1 **Figure 4.** Comparison of CIMEL and UVMFR retrieved AODs for synchronous
2 measurements for 332 nm (up) and 368 nm (down).

4

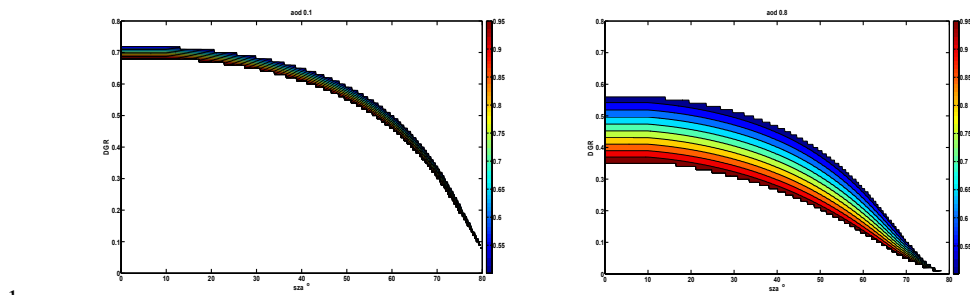
5 The results of this comparison have a Pearson product moment correlation coefficient equal to
6 0.96 and 0.98 respectively for 332nm and 368nm AODs. Mean differences were zero, with
7 standard deviations of 0.031 and 0.025 for the respective wavelengths, comparable with the
8 CIMEL AOD retrieval uncertainty of ± 0.02 . The quality of the data produced can be verified
9 by comparing the AOD's retrieved by the two instruments as a function of SZA (figure 4).
10 Stability of the AOD differences as a function of SZA verifies the validity of the calibration
11 of the UVMFR AOD's and the fact that no SZA-dependent errors (that would be directly
12 related with an erroneous ETC determination) are included in this procedure. In figure 5,
13 AOD's have been grouped in bins of 5 degrees (of SZA). The differences shown in figure 5
14 include ETC determination accuracy, the extrapolation of CIMEL AOD at 368nm, together
15 with instrumental/measurement errors. Using a single UVMFR ETC for the whole period
16 provides very good agreement between the two instruments. However, this may not be the
17 case for all UVMFR instruments using this approach as ETC may suddenly or gradually
18 change especially for years-long time series due to instrumental (filter related) changes.
19 AOD's deviations could lead to large errors on SSA calculations, so this comparison ensures
20 that these errors are minimized.



1

2 **Figure 5** AOD differences between CIMEL and UVMFR at 368 nm, as a function of solar
3 zenith angle.

4 We calculated look up tables (LUT) with the RTM, of DGR at 368nm and 332nm as a
5 function of SZA, AOD, SSA, asymmetry factor (g) and total column ozone.
6 CIMEL/AERONET mean daily ozone values and climatological NO₂ values were deployed
7 for the use of the LUT while for g , we used the mean daily value as retrieved at 440nm from
8 the CIMEL instrument measurements when available and the mean value of the whole period
9 equal to 0.7 (2 σ standard deviation of the g during this period was 0.04) otherwise. Using
10 UVMFR AOD and DGR measurements, we then calculated the matching SSA values for each
11 individual UVMFR DGR measurement. LUT examples are visualized in figure 6, for
12 clarification of the method. For known SZA and AOD (in cloudless sky conditions), the
13 variability of the DGR is caused by aerosol properties other than AOD. At low aerosol loads
14 this variation is nearly negligible, but it becomes more important at higher aerosol load. More
15 absorbing aerosols lead to smaller values of DGR. It is crucial to observe the range of SSAs
16 in the two examples. For low AOD's, accurate SSA determination requires very low
17 uncertainty of the DGR and the AOD measurement. While for high AOD's the range of
18 DGRs for a particular SZA is quite large.



1

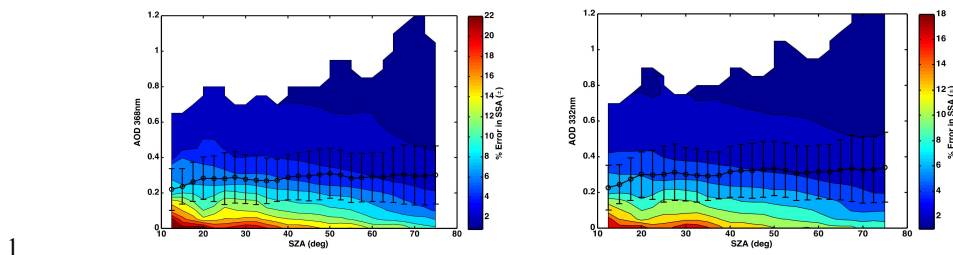
2 **Figure 6** LUT of direct to global ratio at 368nm, as calculated for AOD 0.1 (left)
3 and 0.8 (right) with respect to SZA ($g=0.7$), colourbar represents SSA values.

4

5 **2.3 Retrieval Uncertainties**

6

- 7 The CIMEL sunphotometer provides SSA inversion retrievals characterized as Level 1.5 and
8 Level 2.0 data. Level 2.0 (L2) data are recommended by AERONET as they have less
9 uncertainty but are restricted in measurement to $SZA > 50$ degrees, AOD at 440 nm > 0.4 and
10 homogeneous sky conditions. These limitations make AERONET SSA L2 worldwide
11 measurements unsuitable for:
12 a. climatological studies due to the AOD restriction that limits analyses only to areas having
13 large average annual AOD's, or to cases of moderate to high aerosol episodes in specific
14 areas. As an example, for the urban site of Athens, which is one of the most polluted cities in
15 Europe, the number of measurements is limited to an average 11 cases per month for the
16 whole analysis period.
17 b. diurnal variation studies due to the SZA restriction. For mid and low latitude sites, this
18 limitation leads to a severe lack of information on diurnal SSA patterns as there are only few
19 wintertime measurements and close to zero measurements at local noon.



1 **Figure 7** Uncertainty estimate (color) for the SSA retrieval from UVMFR as a function of
2 AOD and solar zenith angle for 368nm (left panel) and 332nm (right panel), based on DGR
3 and AOD uncertainties. Superimposed, mean AODs for 2.5 degree bins of solar zenith angle
4 are shown.
5

6

7 Level 1.5 data: AERONET Level 1.5 (L1.5) SSA data are provided by AERONET for all
8 AOD's and at all SZA that almucantar scans are performed. In this work L1.5 data were used,
9 but with an extra quality control. We have ignored SSA L1.5 data when L2 size distribution is
10 not available. Thus we have an enhanced L1.5 SSA data set with AOD<0.4, but with L2 cloud
11 screening, calibrations and quality controls. Data has been compared with UVMFR retrieved
12 SSA's taking into account limitations related with the retrieval uncertainties. Khatri et al
13 (2016) studied AERONET SSA retrieval uncertainties, in order to compare with SKYNET
14 and found that AOD errors introduce the largest variations. They also found that the sky
15 irradiance calibration has a primary role on the uncertainty of the retrieval, and they
16 investigated influence of surface albedo and sphericity of aerosols, that was found negligible.

17 For the UVMFR data the uncertainty of the UVMFR SSA retrieval is mainly related to:

- 18 - direct to global irradiance measurements uncertainties.
19 - RTM input data accuracy.

20 Direct to global irradiance measurement uncertainties can result to a range of SSA values
21 rather than a single value, that would produce a match between the measurement and the
22 RTM DGR outputs. This range broadens at low SZA and low aerosol level cases. The RTM
23 inputs that were used for the SSA LUT construction include also an uncertainty budget
24 (AOD, surface albedo, constant aerosol vertical profile, asymmetry factor). Following the
25 uncertainty analysis of Krotkov et al. (2005b), the total relative uncertainty of the DGR
26 measurement was calculated to be $\pm 3\%$. AOD uncertainty is considered as $\pm 2\%$ for 368nm

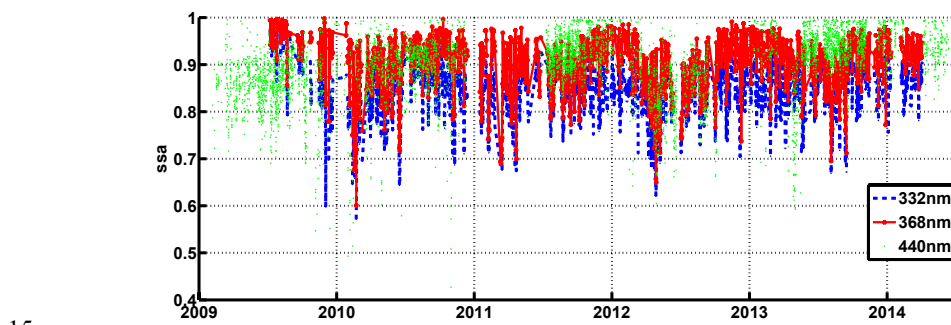


1 and $\pm 4\%$ for 332nm, following the analysis of previous section. The impact of this on the
2 SSA calculation is directly connected with AOD levels and the SZA. In figure 7 we have
3 calculated the UVMFR SSA retrieval uncertainty for different AOD's and solar zenith angles,
4 caused by DGR and AOD uncertainty. DGR and AOD uncertainty ranges from previous
5 paragraph were used to calculate the possible SSA range and the expected error. In the same
6 figure, the mean AOD's and 1σ , for Athens measured by the UVMFR at each solar angle, are
7 shown.

8

9 **3 SSA retrieval results**

10 Using the methodology described in the previous section we calculated the SSA at 332nm and
11 368nm using 1 minute data from the UVMFR. For the period under investigation, we also
12 calculated the daily mean SSA's at these two wavelengths in the UV band and also the mean
13 daily SSA's in the visible band derived from data provided by the CIMEL (L1.5 data)
14 operating in Athens' AERONET station (figure 8).



15
16 **Figure 8** Mean daily SSAs in the UV (UVMFR) at two wavelengths and the visible range
17 (CIMEL) for Athens area.

18

19 The variability of SSA during this period is quite high, ranging from 0.75 (0.62) to 0.98 (0.97)
20 for 332nm (368nm) (2 standard deviations) with mean values of 0.90, 0.87 and 0.83 for
21 440nm, 368nm and 332nm respectively. In figure 9 we have calculated the mean monthly
22 values of SSA at UV wavelengths and standard deviations for the whole period to examine
23 the annual variability. The lowest SSA values were found for the period from February to
24 May at both wavelengths, which should be linked to the usual dust events during this period



for the specific area, and also the presence of brown carbon. Pareskevopoulou et al (2014), have found maximum values of Organic and Elemental Carbon, at February and November, at a 5 year (2008-2013) data set of in-situ measurements, at center of Athens. However, most months have similar behavior, with differences that lie well within the SSA variability of each month.

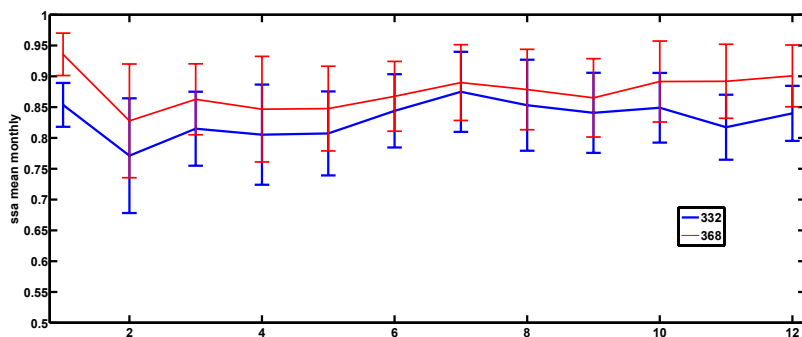
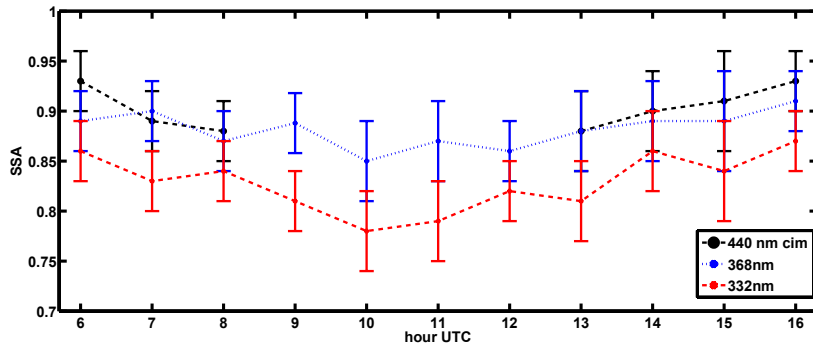


Figure 9 Mean monthly SSAs in the UV (UVMFR) at two wavelengths for the whole 5-year period, at Athens, errorbars at 1σ .

When calculating diurnal patterns of the SSA at UV and visible wavelengths for the Athens area, we observed a mean diurnal pattern with a variability of the order of 0.02 to 0.05 and having highest absorption (lowest SSA's) ± 2 hours around noon (figure 10). Similar behavior can also be seen from AERONET retrieved SSA's having higher values observed during the early morning and late evening. However, the SZA limitation of the AERONET retrieval methodology leads to lack of measurement points around noon. To investigate the uncertainty in relation to UVMFR retrievals, the diurnal pattern was calculated for different SSA uncertainty bins according to the analysis of the previous section. In general, the daily pattern is clear for each bin and is mirrored by the AERONET inversion retrievals. However, the statistical error bars describing the variability of the SSA's during each hourly bin, are quite large.

21



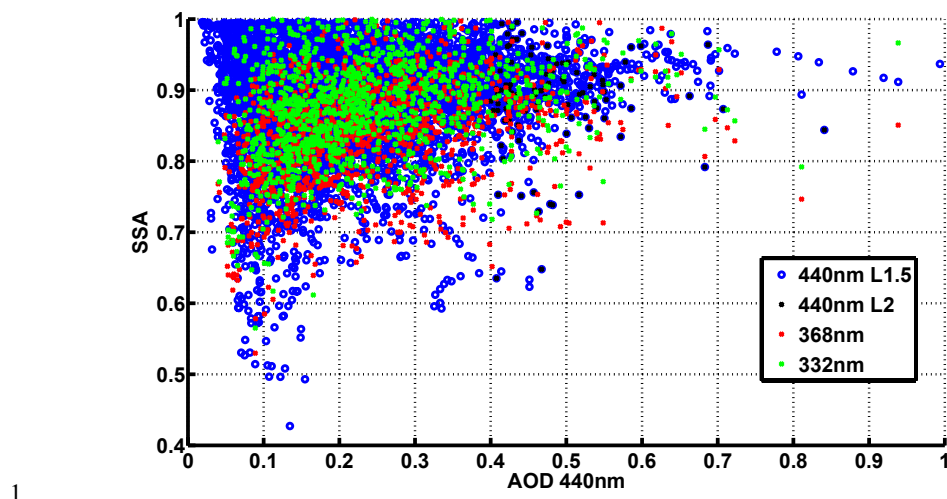
1 **Figure 10** Diurnal patterns of SSA derived from the UVMFR and CIMEL measurements.

2 Mean values per hour plotted at 1σ . Local time in Athens is UTC+2(winter) UTC+3(summer)

3

4

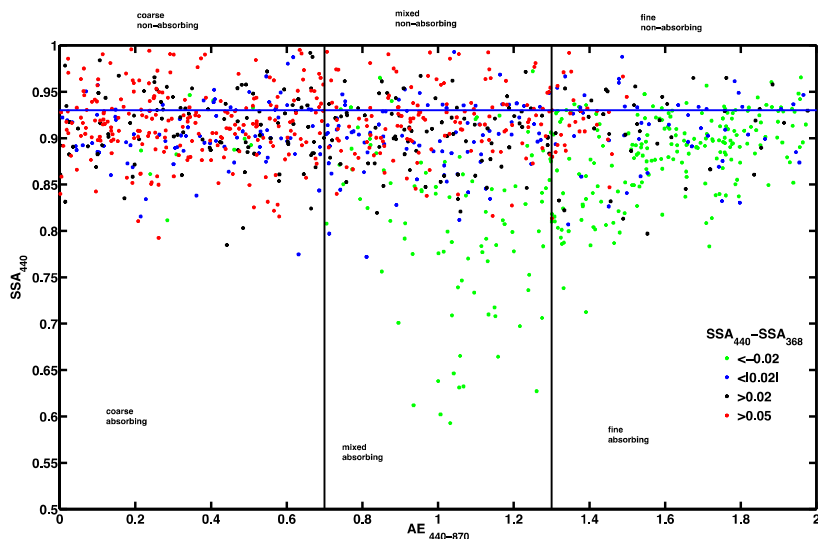
5 In order to investigate the possible dependence of SSA on AOD, figure 11 shows the
6 synchronous UVMFR and CIMEL SSA retrievals plotted against AOD at 440nm. We found
7 that in general, SSA decreases with a decrease in optical extinction, although lower AOD's
8 are linked to higher uncertainties of retrieved SSA. We believe that this behavior reflects
9 seasonal changes in the average aerosol composition in Athens. Indeed, the annual cycle of
10 SSA is the same as the AOD annual cycle having a maximum in summer and a minimum in
11 winter. Studies of the SSA annual variability for other cities such as Ispra, Italy and
12 Thessaloniki, Greece (Arola et al., 2005, Bais et al., 2005) revealed the same trend, with low
13 SSA values (high absorption) associated with low AOD and reminiscent of mostly wintertime
14 cases. It has to be noted that due to low AOD, uncertainties associated with the data obtained
15 from both retrieval techniques (AERONET and UVMFR), are quite high. For higher AOD,
16 CIMEL retrievals show an almost constant value of the SSA ~ 0.92 while lower values have
17 been calculated when moving towards shorter wavelengths. Similar results were reported by
18 Krotkov et al. (2005b) when analyzing measurements derived at Washington, USA.



1
2 **Figure 11** Dependence of the calculated SSA from AOD measurements
3

4 We performed an analysis of the differences of SSAs between the visible and the UV parts of
5 the spectrum based on aerosol characteristics using synchronous CIMEL and UVMFR SSA
6 retrievals and an aerosol classification scheme described in detail in Mielonen et al. (2009).
7 There, a classification of AERONET data was used in order to derive 6 aerosol types based
8 on the SSA measurement at 440nm and the AE that was derived in the 440-870 nm
9 wavelength range. Mielonen et al. (2009) used a visualization of this characterization, by
10 plotting AE versus SSA for individual sites, and compared their results with the CALIPSO
11 (Omar et al., 2005) aerosol classification scheme obtaining good agreement. In addition, the
12 difference between SSA at 440 nm and 1020 nm (similar to the approach applied by Derimian
13 et al. (2008)), was implemented to better distinguish fine absorbing aerosols from coarse ones.
14 The main idea was to fill this SSA versus AE aerosol type related “space” with the differences
15 of $\text{SSA}_{440}-\text{SSA}_{368}$ (SSADIFF) to investigate a possible link between wavelength dependence
16 and aerosol type. In figure 12 using the Mielonen et al. (2009) aerosol typing approach, we
17 plot SSADIFF for different classes (colored scale), and separate aerosol types by areas in the
18 SSA/AE plot . In addition, actual points of SSA_{440} retrieved by the CIMEL instrument are
19 shown in order to categorize Athens results according to the classification scheme.

20

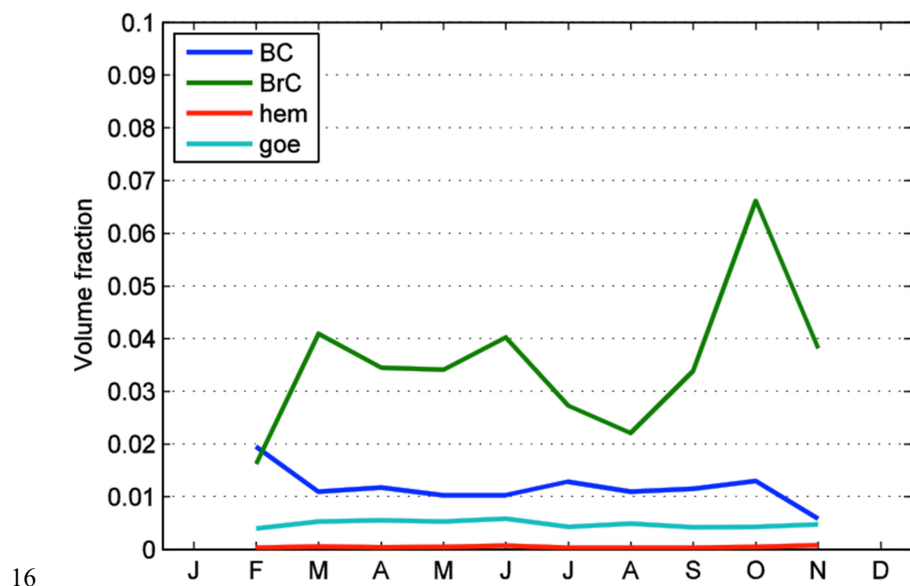


1 **Figure 12** Daily average SSA_{440} (CIMEL) versus $\text{AE}_{(440-870\text{nm})}$. Colors represent different bins
2 of the spectral differences of $\text{SSA}_{440\text{nm}} - \text{SSA}_{368\text{nm}}$.
3
4

5 The results of figure 12 show that a mixture of aerosol types characterizes the ARSS site in
6 Athens, with SSA_{440} values spanning all 6 sub-spaces. Analyzing the wavelength dependence
7 of the SSA, by defining SSADIFF as the difference $\text{SSA}_{440} - \text{SSA}_{368}$, there is evidence that
8 high negative SSADIFF values (that means that the SSA at UV wavelengths is equal or
9 relatively higher than SSA_{440}) tend towards high AEs. For these cases (green color in figure
10 11) we observe high absorption cases with AE's around 1, which can be attributed in polluted
11 dust aerosol events. Also the majority of cases which comply with the condition $\text{AE} < 0.7$ are
12 found with lower SSA at UV by at least 0.05 compared to SSA_{440} . More specifically, dust
13 cases (mainly during spring) can be identified due to the proximity of Athens to the Saharan
14 desert (Gerasopoulos et al., 2010), explaining this behavior of absorbing aerosols at UV with
15 low AE. Russel et al., (2010) reported results obtained from diverse datasets showing SSA
16 wavelength dependency from the IR down to visible wavelengths. In addition, Bergstrom et
17 al. (2007) presented SSA spectra for dust-containing aerosols campaigns (PRIDE and ACE-
18 Asia) including AERONET measurements at sites that are affected by dust such as Cape
19 Verde, Bahrain (Persian Gulf) and the Solar Village (Saudi Arabia). Both studies concluded
20 that the SSA spectra for AERONET locations, dominated by desert dust decrease with
21 decreasing wavelength. In addition, Russel et al., (2010) reported that SSA spectra for



1 AERONET locations dominated by urban-industrial and biomass-burning aerosols decrease
2 with increasing wavelength in line with the results of Bergstrom et al. (2007). Figure 11 also
3 shows that similar SSA values can be found for 440nm and 368nm and for fine aerosol cases
4 ($AE > 1.4$).
5 In order to understand the potential relative contributions of dust and brown carbon better, we
6 applied the method of Schuster et al. 2016 to the AERONET measurements in Athens. This
7 method separates black carbon, organic carbon, hematite and goethite, using refractive index
8 at all available wavelengths, even in complex mixtures. Figure 12 shows the fractions of total
9 aerosol volume attributed to these components in both fine and coarse mode, as well as the
10 volume fractions accordingly. It is evident, according to this approach, that both brown
11 carbon and mineral dust are likely absorbing components involved in the aerosol mixture in
12 Athens, and brown carbon playing the more dominant role. Brown carbon highly absorbs in
13 UV wavelengths and hardly any above 0.7nm (Kirchstetter et all, 2004). BrC fraction is
14 higher at OCTOBER, but it has very large concentrations at the period March-June, which
15 partly explains low SSA values at figure 9.

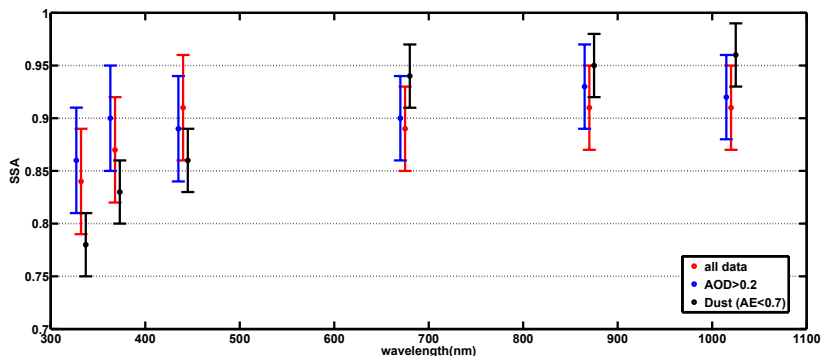


16
17 **Figure 13.** Volume fraction (in the lower plot) of absorbing aerosol components, as inferred
18 by the method of Schuster et al. 2016. The retrieval gives the fractions for fine and coarse
19 mode separately and here the contributions are shown as mode-weighted median value.



1 The utility of the AE for aerosol scattering is that its value depends primarily on the size of
2 the particles, ranging from a value of 4 for very small particles (Rayleigh scattering) to
3 around 0 for very large particles (such as cloud drops). Thus AE for atmospheric aerosol
4 scattering varies between limits specified by particle size. Various studies (e.g. Bergstrom et
5 al., 2007) have used the Ångström Absorption Exponent (AAE) for studying the aerosol
6 absorption wavelength dependence for different aerosol types and mixing (which is calculated
7 similarly with the Ångström Exponent, only using Absorption Optical depth [AOD*(1-SSA)]
8 instead of AOD). As the absorption AOD is a relatively smooth decreasing function with
9 wavelength, it can be approximated with a power law wavelength dependence via the AAE
10 which is defined as the negative of the slope of the absorption on a log-log plot. Figure 13
11 shows the temporal variability of $\text{AAE}_{(440-870)}$ and $\text{AAE}_{(332-440)}$. Measurements of $\text{AAE}_{(440-870)}$
12 are found to lie between 0.9 and 1.5 (2σ) in accordance with the results of Bergstrom et al.,
13 (2007). $\text{AAE}_{(332-440)}$ in the UV range is very different from that in the visible, with values
14 ranging from 1.4 to 5 (2σ). A direct comparison reveals that for the aerosol composition
15 features of Athens, the AAEs are usually up to 4 times higher in the UV range than in the
16 visible. This is due to a combination of the enhanced absorption (lower SSA's) that has been
17 found in the UV, together with higher AOD's in this band.

18 Finally, we have calculated mean CIMEL SSA values for all four retrieved wavelengths
19 (440nm, 673nm, 870nm and 1020nm) for the whole period under study, and synchronous (5
20 minute SSA averaged around the CIMEL measurement time) UVMFR SSAs at UV (332nm
21 and 368nm). The results are shown in figure 14 with errorbars at 1σ . Datasets of SSA
22 retrievals are separated in 3 cases accordingly: a) all points (CIMEL L1.5 and all synchronous
23 UVMFR data), b) measurements retrieved with $\text{AOD} > 0.2$ (reduced uncertainty), and c) SSA
24 retrievals for $\text{AE}_{340-440} < 0.7$, to identify dust events. While for all cases the calculated standard
25 deviation is quite high (≥ 0.05), there is a systematic SSA decrease in the UV range, and mean
26 differences of 0.07 and 0.02 have been found when comparing SSA at the visible range and
27 SSA at 332nm and 368nm respectively. Dust cases in particular show a spectral decrease in
28 SSA with decreasing wavelength from 1022nm (CIMEL) down to 332nm (UVMFR).



1

2 **Figure 14** Wavelength dependence of SSA from synchronous CIMEL and UVMFR
3 measurements. Blue points represent all data points, red data retrievals with AOD>0.2 and
4 black data only dust aerosol cases.

5

6 The spectral dependence of the SSA from the visible to the UV wavelengths is in agreement
7 with findings presented by Corr et al., (2009). With the same approach applied to Mexico City
8 where measurements are also influenced by city emissions and blowing dust, Corr et al.
9 (2009) studied the SSA behavior at UV wavelengths and showed that for AOD>0.1, SSA
10 varied from 0.78 to 0.80 for 332nm and 368nm respectively with enhanced absorption at UV
11 wavelengths relative to the visible wavelengths attributable to these types of aerosols.

12

13 **4 Conclusions**

14 Advantages of measuring the aerosol absorption (SSA) in the UV with the UVMFR
15 instrument can be summarized as follows:

- 16 • AOD, in the UV wavelength range, is higher (for the same aerosol mass) than in the
17 visible spectral range
- 18 • SSA retrievals with the uncertainty of ± 0.03 can be derived for SZA> 40 degrees and
19 with an uncertainty of ± 0.04 for all SZA where AOD ≥ 0.2
- 20 • SSA retrievals are stable and repeatable over the five year period
- 21 We have analyzed a 5 year period of UVMFR and CIMEL measurements at the city of
22 Athens retrieving SSA at visible and UV wavelengths based on the effect of aerosol SSA on



1 the Direct to Global Ratio (DGR) for a given AOD and air mass. Since the CIMEL retrieval
2 algorithm is more accurate for high SZA, the combination of the two instruments allows for
3 an increase in measurement frequency of SSA and the ability to derive a complete diurnal
4 cycle of aerosol absorption. In addition, the spectral differences of the aerosol absorption
5 properties in the visible and UV wavelength range have been investigated, using synchronous
6 CIMEL and UVMFR retrievals. Results of this work confirmed similar results found for
7 Mexico City, Mexico (Corr et al., 2009), Washington DC, USA (Krotkov et al., 2005b) and
8 Rome, Italy (Ialongo et al., 2010), that presented enhanced absorption of aerosols for UV
9 wavelengths.

10 We have also produced dataset to investigate possible effects of aerosol type on observed
11 SSA wavelength differences. The enhanced UV absorption can be mainly due to either dust or
12 organic aerosol. Our analysis of Athens AERONET measurements suggests that the relative
13 role of absorbing organic aerosol would be somewhat more significant than dust. The
14 enhanced aerosol absorption found when comparing UV and visible spectrum results, shows
15 that:

- 16 • We expect a systematic overestimation of modeled solar UV irradiance using SSA
17 from extrapolation from the visible range as an input to RTMs
- 18 • We expect a possible decrease in specific days/cases of regional O₃ due to the
19 enhanced aerosol absorption
- 20 • Satellite post-correction validation results, including aerosol absorption effects, have
21 to take into account absorption enhancement in the UV range.
- 22 • We expect an overestimation on the UV irradiance (UV Index) calculations on
23 cloudless cases under dust and/or brown carbon presence when using SSA values from
24 the visible range. This as a combination of the overestimated SSA and the high AODs
25 during such events.

26 However, the spectral SSA differences, that we found, are well within the uncertainty of both
27 retrievals as instrumental effects or absolute calibration uncertainties of sky radiances (~5%
28 for the CIMEL almucantar measurements) might also play an important role when performing
29 such comparisons. The coincidence of AOD measurements, from both instruments, using a
30 single ETC for various SZA over the extended 5 year period used here, is a sign that no
31 systematic SZA dependent factors influence the final SSA results.



1 The extended SSA dataset significantly improves comparative statistics and provides
2 additional information on the effect of varying background aerosol conditions and higher
3 aerosol absorption than that provided by Washington, DC. In conclusion, the combined use of
4 CIMEL sun and sky radiance measurements in the visible with UVMFR total and diffuse
5 irradiance measurements in the UV, provide an important advantage for remote measurements
6 of column aerosol absorption over the UV-Visible spectral range.

7

8 **Acknowledgements**

9 P.Raptis would like to acknowledge the project «Aristotelis- SOLAR (50561), Investgation on
10 the factors affecting the solar radiation field in Greece». V. Amiridis and S. Kazadzis would like
11 to acknowledge the project “European Union’s Horizon 2020 Research and Innovation
12 Programme ACTRIS-2 (grant agreement no. 654109)”

13

14 **References**

- 15 Alfaro, S. C., Lafon, S., Rajot, J. L., Formenti, P., Gaudichet, A., and Maillé, M.: Iron oxides
16 and light absorption by pure desert dust: An experimental study, Journal of Geophysical
17 Research D: Atmospheres, 109, D08208 08201-08209, 10.1029/2003jd004374, 2004.
- 18 Amiridis, V., Kafatos, M., Perez, C., Kazadzis, S., Gerasopoulos, E., Mamouri, R. E.,
19 Papayannis, A., Kokkalis, P., Giannakaki, E., Basart, S., Daglis, I., and Zerefos, C.: The
20 potential of the synergistic use of passive and active remote sensing measurements for the
21 validation of a regional dust model, Annales Geophysicae, 27, 3155-3164, 10.5194/angeo-27-
22 3155-2009, 2009.
- 23 Arola, A., Kazadzis, S., Krotkov, N., Bais, A., Gröbner, J., and Herman, J. R.: Assessment of
24 TOMS UV bias due to absorbing aerosols, Journal of Geophysical Research D: Atmospheres,
25 110, 1-7, 2005.
- 26 Bais, a F., McKenzie, R. L., Bernhard, G., Aucamp, P. J., Ilyas, M., Madronich, S., &
27 Tourpali, K. (2014). Ozone depletion and climate change: impacts on UV radiation.
28 Photochemical & Photobiological Sciences : Official Journal of the European Photochemistry
29 Association and the European Society for Photobiology. doi:10.1039/c4pp90032d

30



- 1 Bais, A. F., Kazantzidis, A., Kazadzis, S., Balis, D. S., Zerefos, C. S., and Meleti, C.:
2 Deriving an effective aerosol single scattering albedo from spectral surface UV irradiance
3 measurements, *Atmospheric Environment*, 39, 1093-1102 2005.
- 4 Barnard, J. C., Volkamer, R., and Kassianov, E. I.: Estimation of the Mass Absorption Cross
5 section of the organic carbon component of aerosols in the Mexico City Metropolitan Area,
6 *Atmospheric Chemistry And Physics*, 8, 6665-6679, 2008.
- 7 Bergstrom, R. W., Pilewskie, P., Schmid, B., and Russell, P. B.: Estimates of the spectral
8 aerosol single scattering albedo and aerosol radiative effects during SAFARI 2000, *Journal of*
9 *Geophysical Research D: Atmospheres*, VOL. 108, 8474, pp. 11, doi:10.1029/2002JD002435,
10 2003
- 11 Bornman, J.F. and Teramura, A.H. Effects of ultraviolet-B radiation on terrestrial plants. In
12 Environmental UV-Photobiology, Young, A.R., Björn, L.O., Moan, J. and Nultsch, W. (eds.),
13 Plenum Press, New York, pp. 427-471.1993.
- 14 Castro, T., Madronich, S., Rivale, S., Muhlia, A., and Mar, B.: The influence of aerosols on
15 photochemical smog in Mexico City, *Atmospheric Environment*, 35, 1765-1772, 2001.
- 16 Corr, C. A., Krotkov, N., Madronich, S., Slusser, J. R., Holben, B., Gao, W., Flynn, J., Lefer,
17 B., and Kreidenweis, S. M.: Retrieval of aerosol single scattering albedo at ultraviolet
18 wavelengths at the T1 site during MILAGRO, *Atmospheric Chemistry And Physics*, 9, 5813-
19 5827, 2009.
- 20 den Outer, P. N., Slaper, H., and Tax, R. B.: UV radiation in the Netherlands: Assessing long-
21 term variability and trends in relation to ozone and clouds, *J. Geophys. Res.*, 110, D02203,
22 10.1029/2004jd004824, 2005.
- 23 Derimian, Y., J.-F. Léon, O. Dubovik, I. Chiapello, D. Tanré, A. Sinyuk, F. Auriol, T. Podvin,
24 G. Brogniez, and B. N. Holben, Radiative properties of aerosol mixture observed during the
25 dry season 2006 over M'Bour, Senegal (African Monsoon Multidisciplinary Analysis
26 campaign), *J. Geophys. Res.*, 113, D00C09, doi:10.1029/2008JD009904, 2008.
- 27 Dickerson, R. R., Kondragunta, S., Stenchikov, G., Civerolo, K. L., Dodridge, B. G., and
28 Holben, B. N.: The impact of aerosols on solar ultraviolet radiation and photochemical smog,
29 *Science*, 278, 827-830, 1997.



- 1 Diffey, B. L.: Solar Ultraviolet-Radiation Effects On Biological-Systems, Physics In
2 Medicine And Biology, 36, 299-328, 1991.
- 3 Dubovik, O., and King, M. D.: A flexible inversion algorithm for retrieval of aerosol optical
4 properties from Sun and sky radiance measurements, Journal Of Geophysical Research-
5 Atmospheres, 105, 20673-20696, 2000.
- 6 Dubovik, O., B. N. Holben, T. Lapyonok, A. Sinyuk, M. I. Mishchenko, P. Yang, and I.
7 Slutsker, Non-spherical aerosol retrieval method employing light scattering by spheroids,
8 *Geophys. Res. Lett.*, 29(10), 1415, doi:10.1029/2001GL014506, 2002.
- 9 Eck, T.F., Holben, B.N., Reid, J.S., Dubovik, O., Smirnov, A., O'Neill, N.T., Slutsker, I. and
10 Kinne, S., "Wavelength dependence of the optical depth of biomass burning, urban and desert
11 dust aerosols," *J. Geophys. Res.* 104, 31333–31350. 1999.
- 12 Eck T. F., B. N. Holben, I. Slutsker, and A. Setzer, "Measurements of irradiance attenuation
13 and estimation of aerosol single scattering albedo for biomass burning aerosols in Amazonia,"
14 *J. Geophys. Res.* 103, 31865–31878, 1998
- 15 Elminir, H. K.: Sensitivity of ultraviolet solar radiation to anthropogenic air pollutants and
16 weather conditions, *Atmospheric Research*, 84, 250-264, 29 January 2012, 2007.
- 17 Flores, J. M., Washenfelder, R. A., Adler, G., Lee, H. J., Segev, L., Laskin, J., Laskin,
18 A., Nizkorodov, S. A., Brown, S. S., and Rudich, Y.: Complex refractive indices in the
19 near-ultraviolet spectral region of biogenic secondary organic aerosol aged with
20 ammonia, *Phys. Chem. Chem. Phys.*, 16, 10629–10642, doi:10.1039/C4cp01009d, 2014.
- 21
- 22 Gerasopoulos, E., Kokkalis, P., Amiridis, V., Liakakou, E., Perez, C., Haustein, K.,
23 Eleftheratos, K., Andreae, M. O., Andreae, T. W., and Zerefos, C. S.: Dust specific extinction
24 cross-sections over the Eastern Mediterranean using the BSC-DREAM model and sun
25 photometer data: The case of urban environments, *Annales Geophysicae*, 27, 2903-2912,
26 10.5194/angeo-27-2903-2009, 2009.
- 27 Goering, C. D., L'Ecuyer, T. S., Stephens, G. L., Slusser, J. R., Scott, G., Davis, J., Barnard, J.
28 C., and Madronich, S.: Simultaneous retrievals of column ozone and aerosol optical properties
29 from direct and diffuse solar irradiance measurements, *J. Geophys. Res.*, 110, D05204,
30 10.1029/2004jd005330, 2005.
- 31 L. Harrison, J. Michalsky, and J. Berndt, "Automated Multi-Filter Rotating Shadowband



- 1 Radiometer: An instrument for Optical Depth and Radiation Measurements”, Appl. Optics,
2 33, 5118-5125, 1994.
- 3 Gröbner, J., N.Kouremeti, and D.Rembges: A systematic comparison of solar UV radiation
4 spectra with radiative transfer calculations, 8th European Symposium on Physico-Chemical
5 Behaviour of Air Pollutants, A Changing Atmosphere EC, ORA/POST 62172, 2001.
- 6 B. M. Herman, S. R. Browning, and J. J. DeLisi, “Determination of the effective imaginary
7 term of the complex refractive index of atmospheric dust by remote sensing: the diffuse-direct
8 radiation method,” J. Atmos. Sci. 32, 918–925, 1975.
- 9 Holben, B. N., Eck, T. F., Slutsker, I., Tanré, D., Buis, J. P., Setzer, A., Vermote, E., Reagan,
10 J. A., Kaufman, Y. J., Nakajima, T., Lavenu, F., Jankowiak, I., and Smirnov, A.: AERONET-
11 A Federated Instrument Network and Data Archive for Aerosol Characterization, Remote
12 Sens. Environ., 66, 1–16, 1998.
- 13 Ialongo, I., Buchard, V., Brogniez, C., Casale, G. R., and Siani, A. M.: Aerosol single
14 scattering albedo retrieval in the UV range: An application to OMI satellite validation,
15 Atmospheric Chemistry And Physics, 10, 331-340, 2010.
- 16 Kassianov, E. I., Barnard, J. C., and Ackerman, T. P.: Retrieval of aerosol microphysical
17 properties using surface MultiFilter Rotating Shadowband Radiometer (MFRSR) data:
18 Modeling and observations, Journal of Geophysical Research D: Atmospheres, 110, 1-12,
19 10.1029/2004jd005337, 2005.
- 20 Kazadzis, S., Bais, A., Balis, D., Kouremeti, N., Zempila, M., Arola, A., Giannakaki, E.,
21 Amiridis, V., and Kazantzidis, A.: Spatial and temporal UV irradiance and aerosol variability
22 within the area of an OMI satellite pixel, Atmospheric Chemistry And Physics, 9, 4593, 2009.
- 23 Kazadzis, S., Gröbner, J., Arola, A., and Amiridis, V.: The effect of the global UV irradiance
24 measurement accuracy on the single scattering albedo retrieval, Atmos. Meas. Tech., 3, 1029-
25 1037, 10.5194/amt-3-1029-2010, 2010.
- 26 Khatri, P., T. Takamura, T. Nakajima, V. Estellés, H. Irie, H. Kuze, M. Campanelli et al.
27 "Factors for inconsistent aerosol single scattering albedo between SKYNET and AERONET."
28 *Journal of Geophysical Research: Atmospheres* (2016).



- 1 Kirchstetter, T. W., T. Novakov, and P. V. Hobbs, Evidence that the spectral dependence of
- 2 light absorption by aerosols is affected by organic carbon, *J. Geophys. Res.*, 109, D21208,
- 3 doi:10.1029/2004JD004999, 2004.
- 4 M. King and B. M. Herman, "Determination of the ground albedo and the index of absorption
- 5 of atmospheric particles by remote sensing. Part I: Theory," *J. Atmos. Sci.* 36, 163–173. 1979
- 6 M. King, "Determination of the ground albedo and the index of absorption of atmospheric
- 7 particles by remote sensing. Part II: Application," *J. Atmos. Sci.* 36, 1072–1083, 1979
- 8 Krotkov, N. A., Bhartia, P. K., Herman, J., Slusser, J., Labow, G., Scott, G., Janson, G., Eck,
- 9 T. F., and Holben, B.: Aerosol ultraviolet absorption experiment (2002 to 2004), part 1:
- 10 Ultraviolet multifilter rotating shadowband radiometer calibration and intercomparison with
- 11 CIMEL sunphotometers, *Optical Engineering*, 44, 1-17, 2005a.
- 12 Krotkov, N.A., Bhartia, P. K., Herman, J., Slusser, J., Scott, G., Labow, G., Vasilkov, A. P.,
- 13 Eck, T. F., Dubovik, O., and Holben, B. N.: Aerosol ultraviolet absorption experiment (2002
- 14 to 2004), part 2: Absorption optical thickness, refractive index, and single scattering albedo,
- 15 *Optical Engineering*, 44, 1-17, 2005b.
- 16 Krotkov, N. A., Bhartia, P. K., Herman, J. R., Fioletov, V., and Kerr, J.: Satellite estimation
- 17 of spectral surface UV irradiance in the presence of tropospheric aerosols 1. Cloud-free case,
- 18 *Journal of Geophysical Research D: Atmospheres*, 103, 8779-8793, 1998.
- 19 Kudo, R., Uchiyama, A., Yamazaki, A., Kobayashi, E., and Nishizawa, T.: Retrieval of
- 20 aerosol single-scattering properties from diffuse and direct irradiances: Numerical studies, *J.*
- 21 *Geophys. Res.*, 113, D09204, 10.1029/2007jd009239, 2008.
- 22 Liu S, AC Aiken, K Gorkowski, MK Dubey, CD Cappa, LR Williams, SC Herndon, P
- 23 Massoli, EC Fortner, PS Chhabra, WA Brooks, TB Onasch, JT Jayne, DR Worsnop, S China,
- 24 N Sharma, C Mazzoleni, L Xu, NL Ng, D Liu, JD Allan, JD Lee, ZL Fleming, C Mohr, P
- 25 Zotter, S Szidat, and ASH Prévôt, Enhanced light absorption by mixed source black and
- 26 brown carbon particles in UK winter, *Nature Communications*, 6, 8435,
- 27 doi:10.1038/ncomms9435, 2015.
- 28
- 29 Mayer, B., and Kylling, A.: Technical note: The libRadtran software package for radiative
- 30 transfer calculations - Description and examples of use, *Atmospheric Chemistry and Physics*,
- 31 5, 1855-1877, 2005.



- 1 Medina, R., Fitzgerald, R. M., & Min, Q. (2012). Retrieval of the single scattering albedo in
- 2 the El Paso-Juarez Airshed using the TUV model and a UV-MFRSR radiometer. *Atmospheric*
- 3 *Environment*, 46, 430–440. doi:<http://dx.doi.org/10.1016/j.atmosenv.2011.09.028>
- 4 Meleti, C., Bais, A. F., Kazadzis, S., Kouremeti, N., Garane, K., & Zerefos, C. (2009). Factors
- 5 affecting solar ultraviolet irradiance measured since 1990 at Thessaloniki, Greece.
- 6 International Journal of Remote Sensing, 30(15-16), 4167-4179.
- 7 Mielonen, T., Arola, A., Komppula, M., Kukkonen, J., Koskinen, J., de Leeuw, G., and
- 8 Lehtinen, K. E. J.: Comparison of CALIOP level 2 aerosol subtypes to aerosol types derived
- 9 from AERONET inversion data, GEOPHYS. RES. LETT., 36, L18804,
- 10 10.1029/2009gl039609, 2009.
- 11 Moosmüller, H., J. P. Engelbrecht, M. Skiba, G. Frey, R. K. Chakrabarty, and W. P. Arnott
- 12 (2012), Single scattering albedo of fine mineral dust aerosols controlled by iron concentration,
- 13 J. Geophys. Res., 117, D11210, doi:[10.1029/2011JD016909](https://doi.org/10.1029/2011JD016909).
- 14 Müller, D., Wandinger, U., and Ansmann, A.: Microphysical particle parameters from
- 15 extinction and backscatter lidar data by inversion with regularization: Simulation, Applied
- 16 Optics, 38, 2358-2368, 1999.
- 17 Nakajima, T., Tonna, G., Rao, R., Boi, P., Kaufman, Y., & Holben, B. (1996). Use of sky
- 18 brightness measurements from ground for remote sensing of particulate polydispersions.
- 19 Applied Optics, 35(15), 2672-2686.
- 20 Nikitidou, E., Kazantzidis, A., De Bock, V., De Backer, H., The aerosol forcing efficiency in
- 21 the UV region and the estimation of single scattering albedo at a typical West European site,
- 22 Atmospheric Environment (2013), doi: 10.1016/j.atmosenv.2012.12.035
- 23 Omar, A. H., Won, J. G., Winker, D. M., Yoon, S. C., Dubovik, O., and McCormick, M. P.:
- 24 Development of global aerosol models using cluster analysis of Aerosol Robotic Network
- 25 (AERONET) measurements, Journal Of Geophysical Research-Atmospheres, J. Geophys.
- 26 Res. 110: D10S14, doi: 10.1029/2004JD0048, 2005.
- 27 Paraskevopoulou, D., Liakakou, E., Gerasopoulos, E., Theodosi, C., & Mihalopoulos, N.
- 28 (2014). Long-term characterization of organic and elemental carbon in the PM 2.5 fraction:
- 29 the case of Athens, Greece. Atmospheric Chemistry and Physics, 14(23), 13313-13325.



- 1 Paur, R. J., and A. M. Bass. 1985. "The Ultraviolet Cross-Sections of Ozone: II. Results and
- 2 Temperature Dependence." In *Atmospheric Ozone*, edited by C. S. Zerefos and A. Ghazi,
- 3 611– 616. Dordrecht: Springer.
- 4 Petters, J. L., Saxena, V. K., Slusser, J. R., Wenny, B. N., and Madronich, S.: Aerosol single
- 5 scattering albedo retrieved from measurements of surface UV irradiance and a radiative
- 6 transfer model, *Journal of Geophysical Research D: VOL. 108, NO. D9, 4288*,
- 7 doi:10.1029/2002JD002360, 2003.
- 8 Reuder, J., and Schwander, H.: Aerosol effects on UV radiation in nonurban regions, *Journal*
- 9 *of Geophysical Research D: Atmospheres*, 104, 4065-4077,
- 10 Russell, P. B., Bergstrom, R. W., Shinozuka, Y., Clarke, A. D., DeCarlo, P. F., Jimenez, J. L.,
- 11 Livingston, J. M., Redemann, J., Dubovik, O., and Strawa, A.: Absorption Angstrom
- 12 Exponent in AERONET and related data as an indicator of aerosol composition, *Atmospheric*
- 13 *Chemistry And Physics*, 10, 1155-1169, 10.5194/acp-10-1155-2010, 2010.
- 14 Schuster, G. L., Dubovik, O., & Arola, A. (2016). Remote sensing of soot carbon – Part 1 :
15 Distinguishing different absorbing aerosol species, 1565–1585. doi:10.5194/acp-16-1565-
16 2016
- 17 Tanskanen, A., Lindfors, A., Määttä, A., Krotkov, N., Herman, J., Kaurola, J., Koskela, T.,
18 Lakkala, K., Fioletov, V., Bernhard, G., McKenzie, R., Kondo, Y., O'Neill, M., Slaper, H.,
19 den Outer, P., Bais, A. F., and Tamminen, J.: Validation of daily erythemal doses from Ozone
20 Monitoring Instrument with ground-based UV measurement data, *Validation of daily*
21 *erythemal doses from ozone monitoring instrument with ground-based UV measurement*
22 *data*,~*J. Geophys. Res.*, 112, D24S44, doi:10.1029/2007JD008830, 2007
- 23 Taylor, T. E., L'Ecuyer, T. S., Slusser, J. R., Stephens, G. L., and Goering, C. D.: An
24 operational retrieval algorithm for determining aerosol optical properties in the ultraviolet, *J.*
25 *Geophys. Res.*, 113, D03201, 10.1029/2007jd008661, 2008.
- 26 UNEP, Van der Leun, J. C., Tang, X., and Tevini, M.: Environmental effects of ozone
27 depletion: 1998 assessment, *Journal of Photochemistry and Photobiology B: Biology*, 46,
28 10.1016/s1011-1344(98)00195-x, 1998.
- 29 UNEP: Environmental effects of ozone depletion and its interactions with climate change:
30 2002 assessment, executive summary, *Photochem. Photobio. S.*, 2, 1–4, 2003.



- 1 UNEP, Van Der Leun, J., Bornman, J. F., and Tang, X.: Environmental effects of ozone
- 2 depletion and its interactions with climate change: 2006 Assessment, Photochem. Photobiol.
- 3 Sci., 2007,6, 209-209, DOI: 10.1039/B700016B. 2007.
- 4 Van Weele, M., Martin, T. J., Blumthaler, M., Brogniez, C., Den Outer, P. N., Engelsen, O.,
- 5 Lenoble, J., Mayer, B., Pfister, G., Ruggaber, A., Walravens, B., Weihs, P., Gardiner, B. G.,
- 6 Gillotay, D., Haferl, D., Kylling, A., Seckmeyer, G., and Wauben, W. M. F.: From model
- 7 intercomparison toward benchmark UV spectra for six real atmospheric cases, Journal of
- 8 Geophysical Research D: Atmospheres, 105, 4915-4925, 2000.
- 9 WMO: Scientific Assessment of Ozone Depletion: 2002. Global Ozone Research and
- 10 Monitoring Project - Report No. 47, Geneva, Switzerland, 498 pp, 2003.
- 11 Yu, H., Kaufman, Y. J., Chin, M., Feingold, G., Remer, L. A., Anderson, T. L., Balkanski, Y.,
- 12 Bellouin, N., Boucher, O., Christopher, S., DeCola, P., Kahn, R., Koch, D., Loeb, N., Reddy,
- 13 M. S., Schulz, M., Takemura, T., and Zhou, M.: A review of measurement-based assessments
- 14 of the aerosol direct radiative effect and forcing, Atmospheric Chemistry And Physics, 6, 613-
- 15 666, 2006.
- 16 Zerefos, C. S., Tourpali, K., Eleftheratos, K., Kazadzis, S., Meleti, C., Feister, U., Koskela,
- 17 T., and Heikkilä, A.: Evidence of a possible turning point in solar UV-B over Canada, Europe
- 18 and Japan, Atmospheric Chemistry And Physics, 12, 2469-2477, 10.5194/acp-12-2469-2012,
- 19 2012.